Unraveling DNA tori under tension

C. Battle,[1,*] B. van den Broek,[2,†] M. C. Noom,[2] J. van Mameren,[2,‡] G. J. L. Wuite,[2] and F. C. MacKintosh[2,§]
[1]*Institute for Theoretical Physics, Universiteit van Amsterdam, 1018 XE Amsterdam, The Netherlands*
[2]*Department of Physics and Astronomy and Laser Center, Vrije Universiteit, 1081 HV Amsterdam, The Netherlands*
(Received 29 April 2009; published 25 September 2009)

Motivated by recent experiments, we develop a model for DNA toroids under external tension. We find that tori are the equilibrium states for our model up to a critical tension, above which they become only metastable. Above this tension, we find a cascade of transitions between discrete toroid states that successively lower the winding number, until the ground state (rod) is reached. In this process, this model predicts a nearly constant force plateau as a function of extension, in agreement with experiment.

DOI: 10.1103/PhysRevE.80.031917 PACS number(s): 87.14.gk, 82.35.Pq, 87.15.−v, 36.20.Ey

I. INTRODUCTION

It has long been recognized that the conformation of polymer chains depends on the solvent properties of the environment [1,2]. In particular, polymers in poor solvent conditions effectively attract each other in an attempt to exclude the solvent, forming collapsed structures that minimize surface contact with the solvent. For flexible polymers, this leads to compact globules of roughly spherical shape, whose kinetic pathway has been shown to involve the formation of a pearl necklace and gradual diffusion of large pearls to the chain end [3–5].

In the case of semiflexible polymers such as DNA, which exhibits a substantial bending stiffness, the energetic penalty for bending causes spherical globules to be energetically disfavored. The apparent equilibrium states for these polymers have been shown to be toroids [6], as these structures balance the tendency for the polymer to condense due to effective polymer-polymer attraction with the tendency to minimize curvature due to bending stiffness. These condensed states have been studied theoretically [7–13], observed in experiments [14–19], and shown by computer simulation [20–24].

In an effort to understand the dynamics of toroid formation, recent experiments have explored the condensation of DNA under tension [25–29]. Motivated by these experiments we analyze theoretically a hierarchy of torus states and explore their equilibrium and metastable structures under tension, as well as transitions between toroid states. We find a sequence of metastable tori under tension. Furthermore, we find that for winding numbers larger than approximately 10, a nearly constant force plateau emerges, which agrees well with recent observations [28,29], as illustrated in Fig. 1.

In Sec. II of this paper, we first define a simple, nonthermal model that incorporates the essential physical effects believed to give rise to DNA toroids: (1) the bending rigidity and (2) the effective attractive interactions between DNA segments, such as the one that can arise in the presence of multivalent ions [6]. We summarize the relevant experiments in Sec. III. We then study the equilibrium and the metastable states of this model, as well as transitions among these states in Sec. IV. We conclude with a discussion of the implications of this model and the relationship of our results to the experiments.

II. MODEL

The first step in examining the equilibrium and the metastable structures of semiflexible polymer condensates under tension is to identify and calculate their energy. We model the conformational energy of a toroid as in Schnurr *et al.* [13], where we assume integer winding number toroids with a single radius of curvature at zero temperature. Our calculations describe a simplified model of tightly packed filaments of vanishing thickness. We do not take into account any winding defects due to topological constraints [30] or

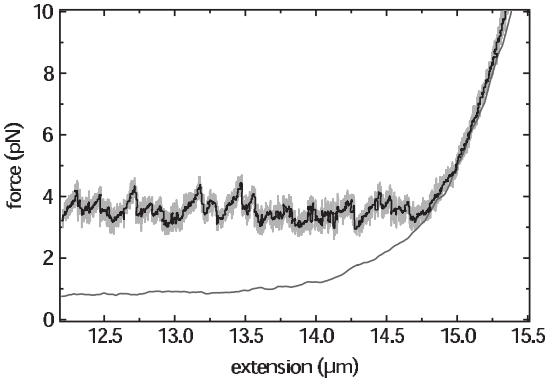

FIG. 1. Measured force-extension curve for condensed DNA from Refs. [28,29]. A lambda-DNA molecule (48 502 base pairs or $\simeq$16.4 μm in length) was stretched using optical tweezers in the presence of spermine 4+ (black line, averaged to 8 Hz, raw data at 128 Hz shown in light gray). In contrast to the force-extension curve of uncondensed DNA (solid gray line), we find a force plateau of approximately 4 pN that persists throughout the curve. In this plateau small steps can be discerned, signifying unwinding of loops from a toroidal DNA condensate.

*Present address: Drittes Physikalisches Institut, Georg-August-Universität, 37077 Göttingen, Germany.
†Present address: Leiden Institute of Physics, Leiden University, 2333 CA Leiden, The Netherlands.
‡Present address: JPK Instruments AG, Bouchestrasse 12, 12435 Berlin, Germany.
§fcm@nat.vu.nl

variations in curvature due to filament thickness.

We write the Hamiltonian of our system as a sum of bending and interaction terms

$$H = H_{bend} + H_{int}, \tag{1}$$

where the bending term models the energy of the curvature of the major radius of the torus and the interaction term models the self-attraction of the polymer or equivalently its poor solvent environment. The bending term can be straightforwardly calculated, as the energy of the idealized chain described is simply that of a series of circular rings, given by [31]

$$H_{bend} = \frac{\kappa}{2}\int_0^L ds\ C^2(s) = \frac{\kappa}{2}\frac{L}{R^2} = \kappa\frac{2\pi^2 N^2}{L}, \tag{2}$$

where $C(s)$ is the curvature, L is the total filament length in the torus, R is the torus radius, $N=L/(2\pi R)$ is the torus winding number, s is the contour length along the filament, and κ is a bending stiffness constant. We note that, since we consider only integer winding number tori, we can write Eq. (2) in terms of a single quantity, L.

For the interaction term, we assume a dense structure, in which filaments pack tightly in their plane perpendicular to their local axis. This suggests a simple hexagonal packing of the filaments. With such tight packing, we assume that the interactions are only of the nearest-neighbor type. In this limit, the filament can be thought of as having six possible binding sites per unit length, which can either form a DNA-DNA bond with another section of the filament or can be exposed to solvent. Bundling occurs when the attractive interactions are sufficiently strong. In order to calculate the interaction term, we define the number of bonds per cross section to be $n_b=(6N-n_s)/2$, where n_s is the number of solvent-exposed sites. We divide by 2 to avoid double counting, as a DNA-DNA bond is equivalent to the merging of two binding sites on neighboring filaments. Our interaction term can thus be written as

$$\begin{aligned} H_{int} &= -\gamma\int_0^{2\pi R} ds\ n_b(s) \\ &= -3\gamma L + \frac{\gamma}{2}\int_0^{2\pi R} ds\ n_s(s) \\ &= -\alpha_1\gamma L + \gamma\frac{\alpha_N}{N}L, \end{aligned} \tag{3}$$

where γ is a surface tension parameter that characterizes the energetic cost of solvent-exposed DNA and α_N is the so-called coordination number [13], which is equal to half the number of solvent-exposed sites per unit length along the torus circumference. We use the coordination number to enumerate these sites, and it can be found by subtracting the number of filament-filament bonds from $3N$. As an example of this scheme, consider the cases $N=5$ and 10: for five filaments there are seven bonds, resulting in a coordination number of 8 (see Fig. 2), while for ten filaments there are 19 bonds, resulting in a coordination number of 11. We then multiply the coordination number by the interaction parameter γ to obtain the surface energy per unit length of a bundle. Table I lists the first 24 coordination numbers. We replace the $3\gamma L$ term in the second line of Eq. (4) with $\gamma L\alpha_1$ to emphasize the physical meaning of this term. The $\gamma\alpha_1 L$ term comes from the difference in surface energy between N strands of unbundled filament and N bundled strands, and it reflects the physical tendency of the torus to minimize unsatisfied bonds through bundling.

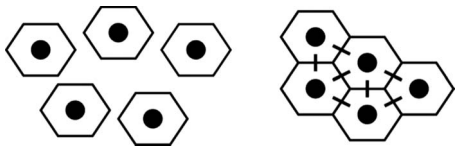

FIG. 2. Sketch of cross section of $N=5$ torus, with hexagonal filament cross section. The perpendicular lines represent bonds between two sites on neighboring filaments.

The packing of filaments in a hexagonal crystal brings about particularly stable toroids for certain winding numbers, as noted previously in Refs. [12,13]. This stability can be attributed to a high degree of hexagonal symmetry and the resulting low surface energy. From Table I we can see that the difference between subsequent coordination numbers α_N is either 0 or 1 (for $N>2$). For instance, in the case of the five-torus bundle shown on the right of Fig. 2, the addition of a sixth filament to the bundle can satisfy no more than two bonds, resulting in no fewer than four additional unsatisfied bonds and an increase in the coordination number by 1. If this sixth filament is added just above the filament on the right, then the addition of a seventh filament directly above the center results in no increase in the coordination number since three bonds can be satisfied. Here, the result is a symmetric compact cross section that we refer to as a *filled shell*. In such cases, where $\alpha_N=\alpha_{N-1}$, we refer to N as a *magic number*, following Refs. [12,13]. Figure 3 shows toroid cross sections for the first seven magic numbers. The magic numbers, up to $N=24$, are as follows: $N=7,10,12,14,16,18,19,21,23,24$. If, instead, $\alpha_N=\alpha_{N-1}+1$, then the smaller $N-1$ torus is favored by both the interaction energy, as well as the bending energy.

As the winding number goes up, we have a higher density of magic numbers. This can be understood by the increase in edge vs corner filaments in the filled shells for large N. For instance, the $N=16$ structure in Fig. 3 can be obtained by

TABLE I. Coordination numbers for tori winding numbers 1–24, with magic numbers in boldface.

Coordination numbers					
α_1	3	α_9	11	α_{17}	15
α_2	5	α_{10}	**11**	α_{18}	**15**
α_3	6	α_{11}	12	α_{19}	**15**
α_4	7	α_{12}	**12**	α_{20}	16
α_5	8	α_{13}	13	α_{21}	**16**
α_6	9	α_{14}	**13**	α_{22}	17
α_7	**9**	α_{15}	14	α_{23}	**17**
α_8	10	α_{16}	**14**	α_{24}	**17**

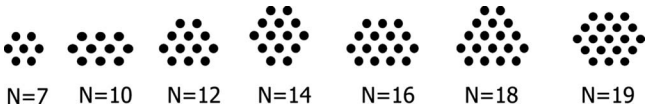

FIG. 3. Sketch of toroid cross sections for the first seven magic numbers. Note that while all have high degrees of symmetry, the $N=7$ and the $N=19$ cross sections correspond to perfect hexagons, and we dub these winding numbers supermagic.

removing three edge filaments from the $N=19$ structure. All but the last one of these filaments satisfy three bonds, corresponding to no change in α, while the final corner filament satisfies only two bonds, corresponding to a reduction in α. Thus, we find sequences of increasing length of successive magic numbers, although equilibrium tori are only found for the largest N in each sequence.

These sequences can be identified as follows. Certain winding numbers correspond to perfect hexagons, such as $N=7$ and $N=19$ in Fig. 3, which we call *supermagic* numbers, as in Ref. [13]. Since these hexagons consist of six equilateral triangles of length $k=1,2,3,\ldots$ filaments on each side plus one filament in the middle of the hexagon, the supermagic sequence is given by $N=3k(k+1)+1$. The coordination number in this case is $\alpha_N=3(2k+1)$. Thus, the difference between successive supermagic α is 6, although the difference in N is $6k$, where k corresponds to the larger N. Hence, the length of each sequence of N with the same coordination number is k, on average. In fact, as suggested by Table I, the actual lengths of the sequences of successive N with equal coordination number are given by $k-1,k,k,k,k,k+1$.

As noted before, semiflexible polymer condensates generically form toroids due to the competition between their tendency to minimize surface area due to short-range attractive forces and their tendency to straighten out due to their substantial bending stiffness. Balancing these two effects, i.e., setting $\kappa/L \sim \gamma L$, lets us define a natural length scale for our problem, which we call the condensation length $L_c = \sqrt{\kappa/\gamma}$. Physically, this length is the approximate length scale at which we expect condensation to occur. Below this length DNA will rarely self-intersect and thus rarely condense, while above it a DNA filament will self-intersect many times and thus form collapsed intermediate structures.

We can also define an analogous energy scale: the condensation energy $U_c=\sqrt{\kappa\gamma}$. Given these scales, we can present our conformational energies in dimensionless units, with physical values of length and energies normalized by their condensation values: $F_N \equiv U_N/U_c$, where U_N is the conformational energy of an N torus, and $\lambda \equiv L/L_c$. The presentation of our results in dimensionless units clarifies the relevant parameters in our theory, namely, the stiffness constant κ and the interaction parameter γ. Combining our expressions for bending and surface energy and normalizing by the condensation energy gives us the dimensionless free energy for an N torus

$$F_N = \frac{2\pi^2 N^2}{\lambda} + \lambda\left(\frac{\alpha_N}{N} - \alpha_1\right). \tag{4}$$

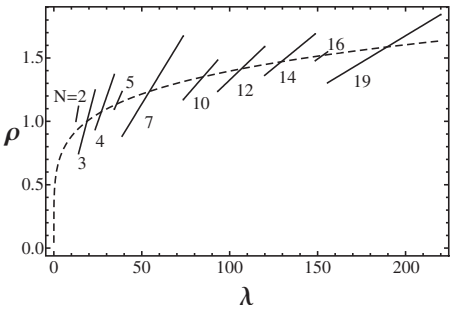

FIG. 4. Plot of reduced radius vs reduced length for equilibrium tori up to $N=19$. The dashed line indicates the prediction based on an approximation valid for large N [9,13]. We note that the minimum size of the first stable torus predicted by this model is $4\pi L_c$. A somewhat smaller length closer to 11 times L_c is found if partial winding of tori is allowed [13].

A. Equilibrium torus states

Plotting Eq. (4) for various N gives a family of curves that tend to negative infinity. While there is no definite global minimum in the free energy for all lengths, for a specific reduced length λ, there is an associated optimal winding number $N(\lambda)$, which corresponds to the equilibrium state at that length. For $\lambda < 4\pi$, the uncondensed rod, $N(\lambda)=0$, is the equilibrium state. From $N=2$ to $N=7$, every state is an equilibrium solution except for $N=6$, which we expect from our discussion of magic numbers. (These results differ somewhat from Ref. [13] since we focus on only tori of integer winding number.)

Above $N=7$, all equilibrium states are magic-number states, although not all magic-number states are equilibrium states. Instead, only the largest in each sequence of consecutive magic-number winding numbers correspond to equilibrium tori in the absence of tension. This can be understood as follows. For $N>12$, the ratio α_N/N, and therefore the interaction energy, has local minima at each value of N such that both $\alpha_N=\alpha_{N-1}$ and $\alpha_{N+1}=\alpha_N+1$. This forms a sequence of winding numbers $N=14,16,19,24,\ldots$ for which particularly stable tori are expected. As can be seen in Table I, these all correspond to magic numbers. Including the effect of bending energy, which always favors smaller winding numbers, consistent with Ref. [13], we find stable tori for this sequence, as well as for the other magic numbers $N=7,10,12$.

It has been noted before [12,13] that the equilibrium radii of the tori do not increase monotonically as a function of reduced length. In fact, as the reduced length is increased, the radii of subsequent equilibrium torus states are marked by discontinuous jumps. Figure 4 shows the reduced radius ρ of the equilibrium states as a function of reduced length, up to $N=19$. The discrete transitions between the radii of different winding numbers are again an effect of the hexagonal packing, which creates islands of stability for certain winding numbers. An equilibrium toroid grows in radius until it reaches a contour length at which the next equilibrium winding number is favored, at which point it transitions to this state. The extra length needed for the additional loops of the higher winding number torus drives the toroid to take on a

smaller radius for the same contour length. For comparison, we also show as the dashed line in Fig. 4 the prediction based on a continuous approximation valid for large N [9,13].

B. Tori under tension

The dimensionless free-energy expression given in Eq. (4) is a measure of the internal energy of the toroid. At zero temperature this is analogous to the Helmholtz free energy of our system. This free energy depends on the reduced length of the filament or the volume of our essentially one-dimensional system. Since we also want to consider the effect of tension, which as a force variable plays the role of pressure in a classical thermodynamics analogy, we perform a Legendre transform on the internal energy of the toroid to get our energy expression in terms of force,

$$E_N = U_N - \frac{dU_N}{dL}L = U_N + fL, \tag{5}$$

where we equate $-dU_N/dL=f$. Here, E_N is analogous to the Gibbs free energy, where tension is the control variable.

The dimensionless form of the Gibbs free energy is obtained again by normalizing Eq. (5) by U_c,

$$G_N = \frac{2\pi^2 N^2}{\lambda} + \lambda\left(\frac{\alpha_N}{N} - \alpha_1\right) + \tau\lambda, \tag{6}$$

where $\tau=f/\gamma$ is the dimensionless tension. Equation (6) represents the dimensionless result for the toroid's conformational energy under tension that we will generally be referring to when we discuss toroidal energy.

III. REVIEW OF EXPERIMENTS

Over the past few years, a number of single-molecule experiments have probed the mechanics of DNA condensation under tension [25–27,32,33]. Generally, in these experiments a single DNA molecule is stretched and relaxed using optical or magnetic tweezers. Under conditions appropriate for condensation, most of these studies reported a nearly constant force plateau of several pN for DNA extensions lower than ~85% of the full contour length. While exact numbers differ between experiments, similar qualitative behavior was observed for a wide range of condensing agents and concentrations.

It has been generally believed that the force plateau regime consists of a continuous unraveling of DNA under tension. In order to test this hypothesis, we measured the force-extension relationship of a single condensed DNA molecule with high resolution using optical tweezers. Lambda-DNA (48 502 bp) was attached on both ends to two optically trapped polystyrene beads [28,29] and allowed to condense in the presence of 1 mM spermine 4+. The condensed DNA was subsequently unraveled by displacing one of the beads. In these experiments, as shown in Fig. 1, the force was allowed to vary freely, while the extension was varied by displacing the trap. We observed a roughly constant force plateau that was consistent with previous experiments. In detail, however, we found that this plateau consists of a sawtooth-like pattern, which suggests a steplike unraveling of the DNA under increasing extension. With the model above, we can account for these discrete steps in terms of jumps between toroid states with different winding numbers. In addition, this model can also account for the nearly constant force plateau. We focus in the present work on the model and its predictions, while the experimental results will be published separately [29].

IV. RESULTS OF THE MODEL

We find that—for finite filament length and zero tension—torus states are, indeed, the equilibrium states within our model, as discussed above. The filament length dictates which torus state has the lowest free energy. For a given filament length λ and winding number N, there exists a finite tension τ_{crit} at which the N torus begins to unravel. For tension $\tau<(\alpha_1-\alpha_N/N)$, the free energy G_N strictly decreases with increasing λ, resulting in a stable or metastable state in which the torus incorporates the full polymer length. Even before this point, however, the free energy $G_N(\tau;\lambda)$ may become greater than zero, indicating that the thermodynamically stable state is the extended polymer conformation. In this case, the tori are actually metastable states.

With increasing tension $\tau>(\alpha_1-\alpha_N/N)$, a local minimum in G_N develops for λ less than the full polymer length. Physically, this corresponds to a mechanical metastable state, or local energy minimum, in which a torus coexists with a segment of unwound straight polymer under tension. The condition for this to occur is

$$\tau > -\frac{\partial F_N}{\partial \lambda}, \tag{7}$$

where the derivative on the right is evaluated at the full polymer length. As the tension increases, more filaments are pulled out of or unwound from the torus, which then shrinks in size. (Here and throughout, we assume that the torus is able to relax by internal relative sliding of polymer.) As the tension increases and the torus shrinks in size, the increased bending energy eventually results in destabilization of the N torus relative to tori of smaller winding number. We identify below a series of transitions under tension to tori of smaller winding number.

A. Transitions

As tension is increased from zero, the slope of the free-energy curve for each N increases. With increasing tension, the $N(\lambda)$ torus initially in equilibrium in the absence of tension for a given total length λ remains the lowest-energy state until a critical tension is reached. At this critical tension τ_{crit}, the asymptotic slope of the free energy becomes zero for large λ. For tensions above this critical tension, the $N(\lambda)$ torus becomes only metastable, as the $(N=0)$ rod is now energetically more favorable (with a free energy of zero) and is thus the equilibrium state of the system. As the tension continues to increase, a local minimum of the free energy develops and starts to shift to lower values of λ. Once this minimum shifts to values of λ less than the full length of the

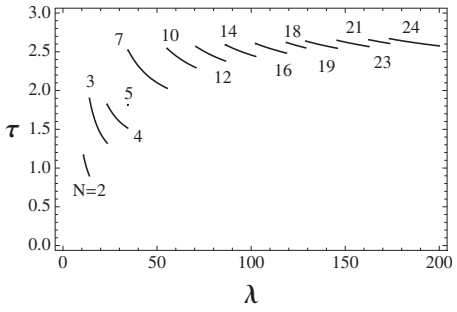

FIG. 5. Tension vs reduced length for preferred tori states from $N=2$ to $N=24$, only plotted at tensions and lengths where we expect them. We note that only magic winding numbers appear for $N>7$ and that a rough force plateau appears at $\tau \approx 2.5$. Transitions between winding numbers are characterized by discontinuous jumps in tension and length.

DNA strand, then the metastable state consists of a compact N torus, with a segment of filament pulled out of the torus—i.e., the torus begins to unravel. With increasing tension, as more of the filaments are pulled out of the torus, larger N tori become unstable to tori with smaller winding numbers. This unraveling process is sequential, with transitions to smaller and smaller values of N as the tension increases.

With an eye toward addressing the experiments in Refs. [28,29], we consider a process in which the reduced length λ in the torus is controlled and slowly reduced, while the tension is allowed to vary. As the N torus is slowly unraveled, the tension τ will increase. However, as τ increases, we expect at some point to develop a local minimum of Eq. (6) for $N-1$ that becomes less than or equal to that of the (metastable) N toroid. Once a transition to the $N-1$ toroid occurs, if the length λ is fixed, then the tension will fall as a new (metastable) $N-1$ toroid is formed at λ. This describes most of the unraveling transitions, at least for large N, where $\alpha_{N-1}=\alpha_N$. However, given the discrete nature of the coordination number α_N, it can happen that the $N-1$ state is itself unstable to the $N-2$ state at λ. This occurs for $N>9$ whenever $\alpha_{N-2}<\alpha_{N-1}$, i.e., when $N-2$ is a magic number. Thus, the $N-1$ state can be expected to make a transition to the $N-2$ state: in the limit of a slow unraveling of the torus, the $N-1$ state is skipped. The resulting sequence of states and the corresponding tensions vs reduced polymer length λ are shown in Fig. 5. Note that the extension of polymer pulled out of the torus varies inversely with λ, meaning that metastable branch corresponds to a stable force-extension relation, in which force increases as more polymer is pulled out of the torus. We find, interestingly, for N greater than about 7, a nearly constant force *plateau* at $\tau \approx 2.5$. This is consistent with several recent experimental observations of a nearly constant force for tori under tension [25,26,28,29], as illustrated in Fig. 1.

The force plateau can be interpreted as the average force needed to pull off a loop from the torus. Since the number of bonds broken when pulling off a loop is either 2 or 3, depending on whether or not the toroid has a magic winding number, it is not surprising that we should see a force plateau at $\tau \approx 2.5$. As we go to higher and higher winding number, however, the force plateau asymptotes to 3. We can see why this is so by considering the average number of bonds per filament as a function of the winding number. In Fig. 6, the most weakly bound filaments are the corner ones, which satisfy only three bonds. The remaining filaments along one edge adjacent to this corner can also be removed at the cost of just three bonds each, until the final corner filament along that edge is reached; the removal of which involves the breaking of just two bonds to form the magic-number bundle with the next lowest coordination number ($N=16$ and $N=33$ for the bundles in Fig. 6). With increasing winding number, the fraction of filaments forming three bonds increases, and $\tau \to 3$, although this convergence is slow.

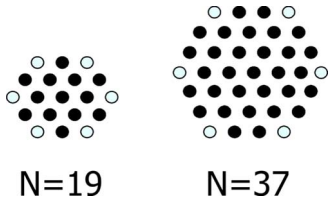

FIG. 6. (Color online) Cross sections of $N=19$ and $N=37$ tori with the lighter circles corresponding to corner filaments. As winding number increases the number of corner filaments always remains six, so the overall density of corner filaments goes down for large N tori.

B. Large N behavior

For large winding number N, the number of exposed unsatisfied bonds at the perimeter of a torus cross section increases as $\sqrt{N}$, so that $\alpha_N \sim \sqrt{N}$. The prefactor here is easy to calculate for perfect hexagons, as illustrated in Fig. 6. As noted in Sec. II, these occur for $N=3k(k+1)+1$, where $k=1,2,3,\ldots$, for which the coordination number is

$$\alpha_N = 3(2k+1) = \sqrt{3(4N-1)}. \tag{8}$$

This actually represents a lower bound on α_N, in general, since less symmetric cross sections have increased surface-to-volume or circumference-to-area ratio. A more rigorous derivation of this bound can be found in Ref. [34]. As we are interested in the large-N behavior, we will approximate

$$\alpha_N \simeq 2\sqrt{3N}, \tag{9}$$

as in Ref. [13].

We use this large-N approximation to determine the metastable states and transitions between them, as we have done in the previous section. Specifically, we consider fixed but decreasing condensed length λ. In Figs. 7 and 8, we indicate the predicted sequence of metastable states and the corresponding values of tension τ and toroid size ρ in reduced units. We find many of the same qualitative features in this large-N approximation as were found in the previous section. In particular, we find an apparent force plateau, much as in Fig. 5. Although both models predict the same asymptotic convergence of the metastable tension $\tau \to 3$ for large λ, where N is also large, we see that the approximate value of α_N from Eq. (9) yields a consistently smaller value of the tension than for the discrete model in Sec. IV A. This can be understood as follows. In the discrete model, we account for

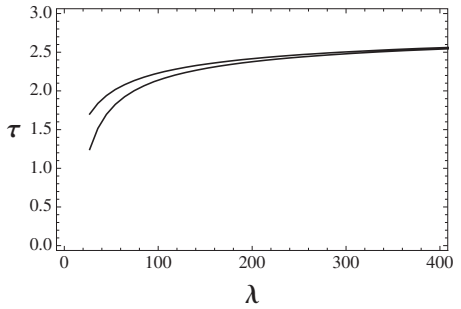

FIG. 7. The range of reduced tensions τ predicted for the metastable states, beginning with the $4 \rightarrow 3$ transition, using the large-N approximation of Eq. (9).

the hexagonal packing of filaments, which results in a sequence of α_N in which there are discrete jumps in α_N (at nonmagic numbers), between which ranges of constant α_N are found. For transitions from N to $N-1$ toroid states, the $N-1$ state is thus destabilized in the discrete model as compared to the large-N approximation, when $\alpha_N = \alpha_{N-1}$. This enhanced relative stability of the N toroid means that the tension τ is larger at the transition. For the same reasons, the corresponding toroid sizes are smaller in the discrete model than in the large-N model. Nevertheless, the general features, and especially the force plateau, are seen for both models.

C. Energy barriers

We estimate the energy barrier between N and $N-M$ tori ($M < N$) first by calculating the energy difference between an N torus and $N-M+M$ tori (see Fig. 9). This is not to suggest that Fig. 9 represents the actual reaction pathway for the transition between tori: calculating the energy in this way, by considering the separation of full loops from the original torus, can only provide an upper bound on the transition energy. From our model, and as suggested by experiment, we expect that toroids make stepwise jumps between different winding numbers.

Intuitively, we expect the transition to depend primarily on the difference in surface area exposed to solvent, and not on the bending energy, since the torus radii vary only weakly with N. In what follows, we shall assume that the radii are constant. We can see from Fig. 9 that the following relations hold since the total amount of the reduced length λ_N is unchanging and all the loop radii are equal: $\lambda_N = \lambda_{N-M} + \lambda_M$, where $\lambda_{N-M} = \frac{N-M}{N}\lambda_N$ and $\lambda_M = \frac{M}{N}\lambda_N$. Here, λ_N is the length in the N torus, λ_{N-M} is the length in the $N-M$ torus, and λ_M is the length in the M torus.

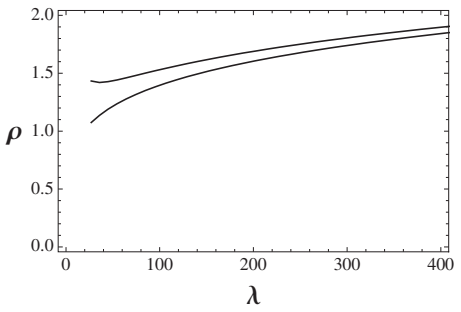

FIG. 8. The range of reduced torus radii ρ predicted for metastable states, beginning with the $4 \rightarrow 3$ transition, using the large-N approximation of Eq. (9).

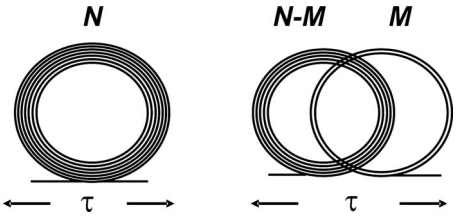

FIG. 9. Sketch of N, $N-M$, and M tori. Physically we expect the energy barrier between these to be dependent only on the surface energy difference, as the bending energy and the tension are unchanged.

With these identifications we can straightforwardly calculate the energy difference between the N torus and the $N-M+M$ tori from the energy expression given by Eq. (6),

$$\Delta E_{N,N-M} = \frac{2\pi^2(N-M)^2}{\lambda_{N-M}} + \lambda_{N-M}\left(\frac{\alpha_{N-M}}{N-M} - \alpha_1\right) + \tau\lambda_{N-M} + \frac{2\pi^2 M^2}{\lambda_M} + \lambda_M\left(\frac{\alpha_M}{M} - \alpha_1\right) + \tau\lambda_M - \frac{2\pi^2 N^2}{\lambda_N} - \lambda_N\left(\frac{\alpha_N}{N} - \alpha_1\right) - \tau\lambda_N = \frac{\lambda_N}{N}(\alpha_{N-M} + \alpha_M - \alpha_N), \tag{10}$$

which depends only on the surface parameters, as expected. We calculate λ_N in the above equation as follows: starting from an N torus we assume downward sequential transitions in the winding number, as previously described, occurring for λ_N where the metastable N and $N-1$ states have equal free energy. For unstable tori, we assume a direct transition to the subsequent winding number at the same value of λ. It is not our purpose to calculate realistic rates of such transitions. Instead, we focus on identifying the most relevant sequence of metastable torus states in a fixed-λ ensemble, corresponding to experiments in which the total length is the control variable. Figure 10 shows the energy barriers be-

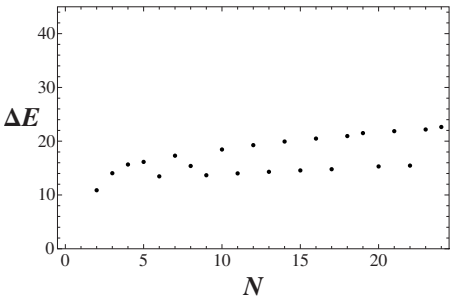

FIG. 10. Estimated energy barriers (dimensionless) vs torus winding number, using Eq. (10), for all N to $N-1$ transitions between $N=2$ and $N=24$. The energy barriers are between N and $N-1$ tori, e.g., the energy barrier plotted at $N=12$ is the energy barrier between $N=12$ and $N=11$.

tween $N \rightarrow N-1$ transitions, from $N=24$ down. We find that transitions from N to $N-M$ for $M>1$ have substantially higher energy barriers and are thereby strongly suppressed.

As noted above, it is unlikely that the transitions sketched in Fig. 9 represent the real reaction pathway between torus states. Nevertheless, our estimates suggest that transitions corresponding to a change in the winding number by more than 1 are strongly suppressed. For $\Delta N=1$, however, it is also possible that DNA peels off continuously from the torus. This will, in general, induce additional bending as the DNA is pulled off the torus. (We assume that twist is relaxed.) In fact, a bend of approximately 90° is expected on simple mechanical grounds since the force in the plateau region in Fig. 5 is comparable to the total binding energy per unit length of filament, as discussed in Sec. IV A. Under a force f, the radius of curvature r for such a bend can be estimated by balancing the total bending energy $\pi\kappa/(4r)$ and the virtual work against the applied tension $(\pi/2-1)rf$. This yields an optimal radius of curvature $r=\sqrt{\pi\kappa/[f(2\pi-4)]}$ and a total energy for two such bends of $\sqrt{\tau\pi(2\pi-4)} \approx 4.2-4.6$ in reduced units for $\tau \approx 2.5-3$. This is about a factor of 2–3 smaller than the estimates from Eq. (10).

Other effects may change the energy barriers as well, such as next-nearest-neighbor interactions. As these interactions are effectively attractive, they will favor more compact structures, thus lowering the length needed for an N torus (i.e., shifting minima in the energy to lower values of λ). This will lower the energy barriers given above for nearest-neighbor interactions, but there will be an additional contribution to the energy barrier from the attraction of next-nearest neighbors that must be overcome to pull off a loop. Without an explicit inclusion of these effects in our model, it is unclear what net effect these interactions will have on energy barriers.

V. DISCUSSION

Of the two parameters in our model, the bending stiffness κ is known to be approximately $\kappa=kT\ell_p \simeq 50kT$ nm, where ℓ_p is the persistence length of DNA. The interaction parameter γ is expected to depend on the counterions present in solution, and it is unfortunately not known. In order to estimate γ, we use the experimentally observed plateau value of the force in Fig. 1. This is consistent with the plateau we find in Fig. 5. By matching the measured force plateau with our (dimensionless) tension $\tau=f/\gamma$, we estimate $\gamma \simeq 1.6$ pN. This is similar to DNA-DNA interaction strengths on the order of a few pN ($\simeq 0.1kT$ per base pair) reported for osmotic stress measurements in Ref. [35], although such measurements were performed under different solution conditions and for different condensing agents. This allows us to estimate the condensation length $L_c \simeq 11$ nm and the condensation energy $U_c \simeq 4.5kT$. This corresponds to energy barriers of order $20kT$, using the lower estimates at the end of Sec. IV C for $\Delta N=1$ transitions. By contrast, we find substantially larger barriers of more than $50kT$ for transitions as sketched in Fig. 9 for $\Delta N>1$.

Figure 5 shows a typical transition length (i.e., the difference in the reduced length between an N torus and an $N-1$ torus at constant tension) of ~ 10, suggesting a typical torus loop size (and also a minimum size of the first stable torus in the absence of tension) of ~ 110 nm, a value larger than that reported in Ref. [29] by a factor of about 2–3. Given the simplicity of our model being off by such a factor is perhaps not so bad, as there are many effects that we have not taken into account. One notable effect that we have neglected is next-nearest-neighbor interactions. Such interactions will have the same attractive tendency as nearest-neighbor bonds and thus will tend to favor more compact structures, translating into smaller loop sizes.

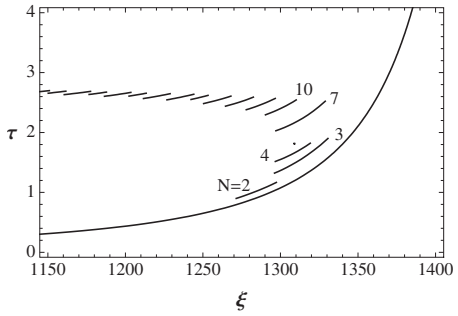

FIG. 11. The predicted force (in units of γ) as a function of the apparent extension ξ (in units of L_c) of DNA toroids in series with freely fluctuating uncondensed DNA. Here, we have used 16.4 μm as the full contour length and $L_c=11$ nm. A few of the individual force-extension curves are labeled by the corresponding winding numbers $N \leq 10$. The thin continuous curve represents the force-extension curve of the bare DNA.

Another possible effect is the stability of the toroids beyond the transition regime. We have predicted the loop sizes from our model assuming immediate transitions once in the transition regime; in reality, toroids may not transition immediately. At higher tensions there are smaller differences in the reduced length between subsequent toroid force-extension curves. If, for example, we instead assume a force plateau at the higher-than-expected value $\tau=3$ (which raises L_c to 12nm), and average over the same range of winding numbers, we get an average step size of $\lambda \simeq 6.5$, translating into a loop size of 78 nm.

One very important effect that must be taken into account in comparing with the measured extensions in the experiments is the finite extensibility of the uncondensed DNA strand, which is expected to be well approximated by a wormlike chain [28,29,36]. We can account for this by considering a thermally fluctuating filament in series with the torus. The length of this filament is equal to the full contour length L_0 of the DNA in the absence of condensation minus the length L contained in the torus. In dimensionless form, the extension $\xi=x/L_c$ of the free DNA in series with the toroid is approximately given by

$$\xi = (\Lambda - \lambda)\left(1 - \frac{kT}{2U_c\sqrt{\tau}}\right), \tag{11}$$

where the full contour length of uncondensed DNA is given by ΛL_c, of which λL_c is contained in the toroid. In Fig. 11 we show the combined force-extension curves of the various

toroid states in Fig. 5, corresponding to $U_c \simeq 4.5kT$ and the full contour length of 16.4 μm in Refs. [28,29]. Interestingly, this model predicts multiple metastable states with winding numbers in the range of approximately 2–10 near the transition to the fully unraveled toroid. This may explain the significant hysteresis reported for forward (extension) and reverse force-extension measurements near the transition between toroid and fully extended DNA [28,29]. As the fully extended state is allowed to condense when reducing the extension, the force drops and toroid states with small N are expected to form at a smaller extension than required, e.g., for the transition from $\simeq 7$ to fully extended DNA.

We have developed a highly simplified model, in which we assume, e.g., perfect hexagonal packing without topological defects, a single radius of curvature in the toroid, and only nearest-neighbor interactions. Nevertheless, this model is able to capture a number of features observed in the experiments. We find that toroid unraveling under tension occurs via a series of discrete transitions, as observed in Refs. [28,29]. In addition, this model provides an explanation for the existence of the approximately constant force plateau for DNA condensations under tension, as reported in a number of experiments [25–29].

[1] P. G. de Gennes, *Scaling Concepts in Polymer Physics* (Cornell University Press, New York, 1979).
[2] M. Doi and S. F. Edwards, *The Theory of Polymer Dynamics* (Clarendon Press, Oxford, 1988).
[3] B. Ostrovsky and Y. Bar Yam, EPL **25**, 409 (1994).
[4] A. Buguin, F. Brochard-Wyart and P. G. de Gennes, C. R. Acad. Sci. Paris, Ser. II **322**, 741 (1996).
[5] B. Chu, Q. C. Ying, and A. Y. Grosberg, Macromolecules **28**, 180 (1995).
[6] W. M. Gelbart, R. F. Bruinsma, P. A. Pincus, and V. A. Parsegian, Phys. Today **53**(9), 38 (2000).
[7] A. Y. Grosberg, Biofizika **24**, 32 (1979).
[8] V. A. Bloomfield, Biopolymers **31**, 1471 (1991).
[9] J. Ubbink and T. Odijk, Biophys. J. **68**, 54 (1995).
[10] V. A. Bloomfield, Biopolymers **44**, 269 (1997).
[11] V. V. Vasilevskaya, A. R. Khokhlov, S. Kidoaki, and K. Yoshikawa, Biopolymers **41**, 51 (1997).
[12] G. G. Pereira and D. R. M. Williams, EPL **50**, 559 (2000).
[13] B. Schnurr, F. Gittes, and F. C. MacKintosh, Phys. Rev. E **65**, 061904 (2002).
[14] A. Z. Li, T. Y. Fan, and M. Ding, Sci. China, Ser. B: Chem. **35**, 169 (1992).
[15] Y. Fang and J. H. Hoh, Nucleic Acids Res. **26**, 588 (1998).
[16] M. R. Shen, K. H. Downing, R. Balhorn, and N. V. Hud, J. Am. Chem. Soc. **122**, 4833 (2000).
[17] A. L. Martin, M. C. Davies, B. J. Rackstraw, C. J. Roberts, S. Stolnik, S. J. B. Tendler, and P. M. Williams, FEBS Lett. **480**, 106 (2000).
[18] D. Liu, C. Wang, Z. Lin, J. W. Li, B. Xu, Z. Q. Wei, Z. G. Wang, and C. L. Bai, Surf. Interface Anal. **32**, 15 (2001).
[19] H. G. Hansma, Annu. Rev. Phys. Chem. **52**, 71 (2001).
[20] H. Noguchi, S. Saito, S. Kidoaki, and K. Yoshikawa, Chem. Phys. Lett. **261**, 527 (1996).
[21] A. Byrne, E. G. Timoshenko, and K. A. Dawson, Nuovo Cimento Soc. Ital. Fis., D **20**, 2289 (1998).
[22] B. Schnurr, F. C. MacKintosh, and D. R. M. Williams, EPL **51**, 279 (2000).
[23] H. Noguchi and K. Yoshikawa, J. Chem. Phys. **113**, 854 (2000).
[24] M. J. Stevens, Biophys. J. **80**, 130 (2001).
[25] C. G. Baumann, V. A. Bloomfield, S. B. Smith, C. Bustamante, M. D. Wang, and S. M. Block, Biophys. J. **78**, 1965 (2000).
[26] Y. Murayama, Y. Sakamaki, and M. Sano, Phys. Rev. Lett. **90**, 018102 (2003).
[27] K. Besteman, S. Hage, N. H. Dekker, and S. G. Lemay, Phys. Rev. Lett. **98**, 058103 (2007).
[28] B. van den Broek, Ph.D. thesis, Vrije Universiteit, Amsterdam, 2007.
[29] B. van den Broek, M. C. Noom, J. van Mameren, C. Battle, F. C. MacKintosh, and G. J. L. Wuite (unpublished).
[30] S. Y. Park, D. Harries, and W. M. Gelbart, Biophys. J. **75**, 714 (1998).
[31] N. V. Hud, K. H. Downing, and R. Balhorn, Proc. Natl. Acad. Sci. U.S.A. **92**, 3581 (1995).
[32] B. A. Todd and D. C. Rau, Nucleic Acids Res. **36**, 501 (2008).
[33] S. Husale, W. Grange, M. Karle, S. Burgi, and M. Hegner, Nucleic Acids Res. **36**, 1443 (2008).
[34] E. L. Starostin, J. Chem. Phys. **129**, 154104 (2008).
[35] D. C. Rau and V. A. Parsegian, Biophys. J. **61**, 246 (1992).
[36] C. Bustamante, J. F. Marko, E. D. Siggia, and S. J. Smith, Science **265**, 1599 (1994); J. F. Marko and E. D. Siggia, Macromolecules **28**, 8759 (1995).